NEUROSCIENCE

Functional representation of trigeminal nociceptive input in the human periaqueductal gray

Jan Mehnert, Alexandra Tinnermann, Hauke Basedau, Arne May*

The periaqueductal gray (PAG) is located in the mesencephalon in the upper brainstem and, as part of the descending pain modulation, is considered a crucial structure for pain control. Its modulatory effect on painful sensation is often seen as a systemic function affecting the whole body similarly. However, recent animal data suggest some kind of somatotopy in the PAG. This would make the PAG capable of dermatome-specific analgesic function. We electrically stimulated the three peripheral dermatomes of the trigemino-cervical complex and the greater occipital nerve in 61 humans during optimized brainstem functional magnetic resonance imaging. We provide evidence for a fine-grained and highly specific somatotopic representation of nociceptive input in the PAG in humans and a functional connectivity between the individual representations of the peripheral nerves in the PAG and the brainstem nuclei of these nerves. Our data suggest that the downstream antinociceptive properties of the PAG may be rather specific down to the level of individual dermatomes.

INTRODUCTION

Located in the midbrain tegmentum, the periaqueductal gray (PAG) is a crucial structure of the descending pain modulatory system (DPMS) (*1*). Activation of this system through the rostro ventromedial medulla (RVM) modulates nociceptive neurons in the dorsal horn of the spinal cord (*2*), controlling nociceptive input into the spinal cord and its subsequent transmission along the ascending pain pathway to thalamus and subsequent regions. The role of the PAG in the DPMS has been extensively studied in analgesic conditions in headache (*3*) and chronic pain (*4*), showing that its electrical (*5*, *6*) and opioidergic (*7*) stimulation recruits the DPMS and results in profound analgesia.

The PAG receives ascending input from the spinal cord and the medullar region (*8*, *9*) and descending input from subcortical and cortical regions such as hypothalamus, amygdala, insula, anterior cingulate, and prefrontal cortex (*10*–*12*). Apart from descending connections to the RVM, the PAG has ascending connections to thalamus, hypothalamus, and orbitofrontal cortex (*13*, *14*).

Research in animals and humans further link PAG activity to defensive behaviors, fear, and thread processing (*9*, *15*–*17*). The cylindrical structure of the PAG is subdivided into four columns (ventrolateral, lateral, dorsolateral, and dorsomedial) (*18*). These columns play different roles during defensive behaviors in animals (*19*) and during threat and aversive emotion processing in humans (*20*, *21*). Moreover, every PAG column is connected to distinct brain networks (*22*), suggesting that each column forms part of a brain circuitry that is responsible for different aspects of these complex behaviors.

Its segregated organization in anatomy and function raises the question whether the DPMS acts pars pro toto or whether it modulates nociceptive input individually for each body part. Clinical experience (for example, the co-occurrence of multiple traumata) suggests that systems modulating pain discriminate down to the level of dermatomes. Benedetti *et al.* (*23*) additionally suggested that the DPMS contains a highly organized and somatotopic network of endogenous opioids. One therefore expects a somatotopic arrangement of the PAG, where individual parts connect to the relay station of attributed dermatomes. Such a somatotopic organization is well known as homunculus (*24*) for sensory and motor cortices. In the context of nociception, somatotopy exists in primary and secondary somatosensory cortex (*25*, *26*), thalamus (*27*), and insula (*28*–*30*). Nevertheless, little literature exists about a somatotopy of the PAG. Moreover, concerning context (pain expectation, etc.) the term DPMS is inherently discussed as a systemic, i.e., holistic, modulation of pain.

Recent research on mammals hints to a somatotopy of the PAG (*31*–*33*): For humans, case reports (*34*, *35*) suggest a rostro-caudally inverted somatotopy with caudal representation of facial and rostral representation of leg stimulation. A recent publication hints for a dominant rostral activation of the PAG during painful stimulation of the head while other body parts seem to be more represented in the caudal part (*36*).

Focusing on the somatotopic representation of nociceptive input in the PAG, we conducted a preregistered (clinicaltrials.gov: NTC03999060) functional imaging study using painful stimulation of the trigeminal and occipital nerves in healthy controls as a model. The trigeminal nerve consists of three branches innervating the forehead and the maxillar and mandibular regions and, together with the occipital nerve, forms the trigemino-cervical complex (TCC) (*37*). This allows precise stimulations of two peripheral nerves and four branches and has the advantage that their first hubs of peripheral input are located within the same imaging frame as the PAG using optimized (*38*) and validated (*39*) brainstem imaging.

RESULTS

Functional somatotopy of the PAG

Painful electrical stimulation on four locations of the left side of the head (Fig. 1B), namely, on the forehead (V1; ophthalmic trigeminal branch), the cheek (V2; maxillar trigeminal branch) the chin (V3; mandibular trigeminal branch), and at the back of the head (GON; greater occipital nerve), was significantly painful ($P < 0.0125$ Bonferroni corrected t tests; average VAS: 57.0 ± 22.6 at V1, 57.2 ± 22.5 at V2, 49.3 ± 23.4 at V3, 56.2 ± 25.4 at GON; $n = 36$). The average

Department of Systems Neuroscience, University Medical Center Eppendorf, 20146 Hamburg, Germany.
*Corresponding author. Email: a.may@uke.de

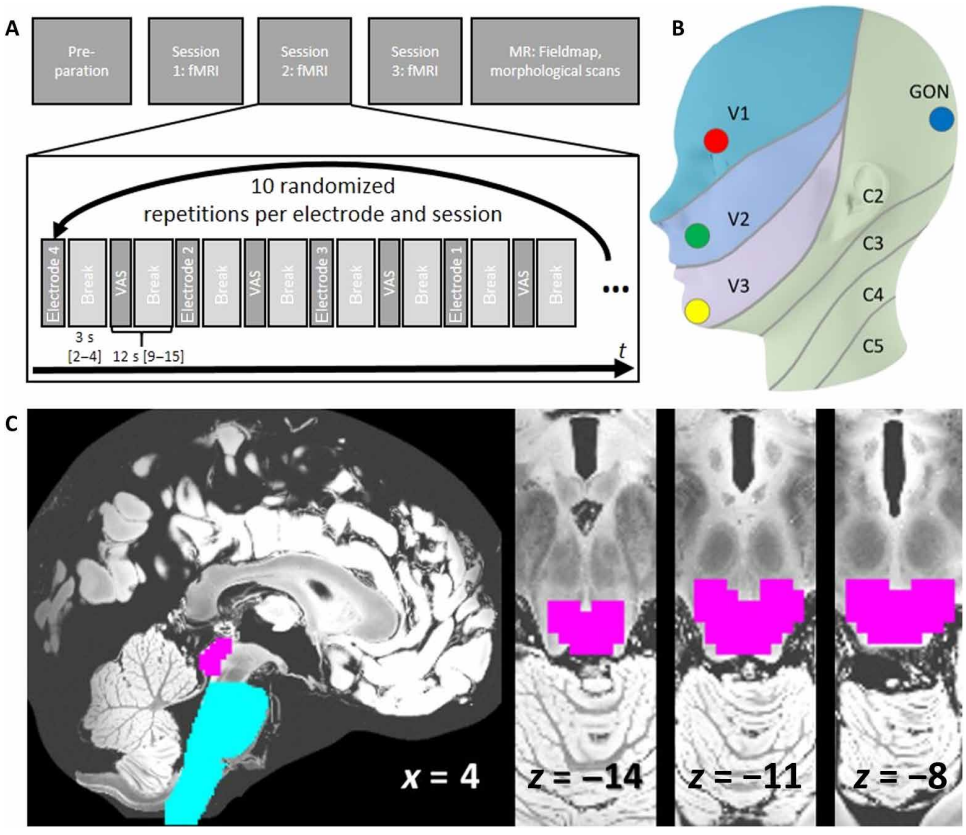

Fig. 1. Experimental design. (**A**) Stimulation sites were randomly presented during three sessions of functional magnetic resonance imaging (fMRI). A break of 3 s (jittered between 2 and 4 s) followed each electrical stimulation after which participants rated the pain intensity on a visual analog scale (VAS) with levels between 0 and 100. The inter-trial interval was set to 15 s (jittered between 12 and 18 s). This results in 30 trials per stimulation site and participant. Morphological scans followed the fMRI. (**B**) The sites for the electrical stimulation are located above the three branches of the trigeminal nerve (V1, V2, and V3) in the participants' face and above the greater occipital nerve (GON) at the back of the participants' head. (**C**) PAG and brainstem masks used for the data analyses.

electrical detection threshold (EDT) was 0.20 mA ± 0.09 and the finally applied current was 1.88 ± 1.15 mA. There were no sex-related differences (Mann-Whitney *U* tests) or correlations (two-sided Spearman's correlation at $\alpha = 0.05$) with age in EDT, final current, and the pain ratings at the individual stimulation sites. All stimulations revealed significant activation of the PAG. Adding sex, age, and EDT as covariates did not change the results. Their activation forms four clusters separated by the predominant activation of the individual stimulation site (Fig. 2). Each cluster of activation has high *t* values reaching from 12.81 to 21.04 [$p_{FWE} < 10^{-4}$, voxel-wise family-wise error (FWE) corrected, $n = 61$, df = 180; Table 1] with higher *t* values on the right side, contralateral to the stimulation. This threshold was achieved in 1395 voxels (54% of the PAG mask). Notably, these clusters are coherent and similar between the hemispheres.

Downstream functional connectivity to the TCC

The exploratory functional connectivity analysis of each cluster in the PAG contralateral to the stimulation site revealed significant connections to the ipsilateral TCC in the lower brainstem, i.e., the first central relay stations of the trigeminal nerve and the greater occipital nerve in the brainstem (Fig. 3). We found a strong functional connectivity to the TCC for the first (106 voxels, *t* value = 4.02, coordinate: [−3, −47, −62]) and the third (29 voxels, *t* value = 3.24, coordinate: [−3, −48, −66]) trigeminal branch as well as for the greater occipital nerve (9 voxels, *t* value = 3.06, coordinate: [−5, −48, −67]) to the ipsilateral (to the stimulation site, i.e., contralateral to the PAG cluster used as seed region) representation in the TCC (Table 2).

DISCUSSION

Using high-precision stimulation of nociceptive trigeminal and greater occipital nerve fibers, our main finding strongly suggests a somatotopic representation of nociceptive input in the PAG in humans. This somatotopic representation is organized down to a dermatome level, given that even the three individual branches of the trigeminal nerve had distinctive representations within the PAG. All four stimulated dermatomes are represented in coherent clusters bilateral of the PAG. The most cranial part of the PAG is mainly represented by the C2/3 or GON dermatome, while V1, V2, and V3, following the peripheral representation, are also represented from cranial to caudal in the PAG. We note that the areas with distinctive representations within the PAG are probably not exclusively representing this single body part but instead represent one body part relatively more than another one. Adding nociceptive input of more body parts will therefore reshape the clusters to a more detailed/fine-grained somatotopy. If the PAG would, as traditionally

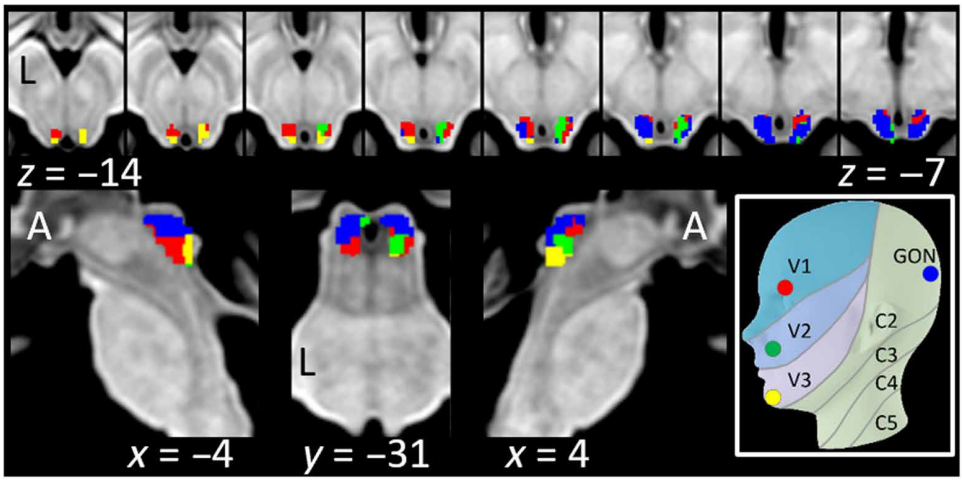

Fig. 2. Somatotopy in the periaqueductal gray. The axial slices of the PAG on top of the figure show the bilateral somatotopy of the individual nerve branches of the trigemino-cervical complex in neurological convention (left is left). On the bottom of the figure, the sagittal view, ipsilateral to the stimulation sites, a coronal slice, and sagittal view, contralateral to the stimulation, are in this order presented. The stimulation sites are marked in the bottom right corner of this figure. Colors represent the individual nerves. V1, ophthalmic branch; V2, mandibular branch; V3, mandibular branch of the trigeminal nerve; C, cervical level; GON, greater occipital nerve; L, left; A, anterior.

considered, have a systemic effect on pain throughout the body, the dermatome-related activity on the PAG would yield a random distribution, i.e., of "winning stimulation sites" in the voxels of the PAG. A similar kind of analysis has just recently been published for the representations of the TCC in the cerebellum (*40*). We find it important to note that also in the motor and somatosensory cortex, within-limb representations widely overlap (*41*–*44*) even in areas where the homunculus is considered dermatome specific. These results echo findings from animal work, which, in a series of experiments, suggested a somatotopic organization in the midbrain (*31*, *45*, *46*) in rostro-caudal arrangement. Human evidence is sparse and only a case report and a case series of another five patients receiving deep brain stimulation also suggested (*34*, *35*) PAG somatotopy. Our findings cannot answer the question whether the PAG activation that we found would functionally inhibit or facilitate nociceptive input, because we did not investigate the antinociceptive response per se. It would, however, not make a difference regarding the question whether the PAG is somatotopically organized. To better delineate the suggested rostro-caudal arrangement of this somatotopy, stimulation of more distant body parts will be necessary.

Our second finding of a significant functional connectivity of the individual clusters within the PAG to the responding brainstem nuclei strongly supports our first finding and also underpins somatotopy of the TCC, although this analysis should be seen as exploratory. Such a somatotopy within the trigeminal nerve has been postulated from animal studies (*47*) and partly also evinced in humans (*48*). Together, this defines possible sites of action for the dermatome-specific analgesic effect of the PAG, which may play an import role in numerous primary headache disorders (*37*). It is, for example, well known that a blockage of the GON leads to a relief in certain headaches like cluster headache (*49*), trigeminal neuralgia (*50*), and probably also migraine (*51*). Recent evidence suggests that the electrical stimulation of the GON may also lead to such an effect (*52*) and that the site of action for this phenomenon lies in the TCC (*53*, *54*).

From an evolutionary-biological standpoint, one would expect the DPMS to be organized similar to the ascending pain system, i.e., highly distributed and in a position to facilitate or block nociceptive input with high local precision. If the ankle is damaged, it does not make sense to uncouple nociceptive input from the rest of

Table 1. Main effect of the cluster analysis in the periaqueductal gray (PAG). Each trigeminal branch (V1, V2, and V3) and the greater occipital nerve (GON) formed one cluster on each side of the PAG (i.e., right versus left) when clustering each PAG voxel according to the stimulation site with maximal activity (i.e., *t* value). The cluster extent refers to the number of contiguous voxel where a stimulation site has the highest *t* value as compared to the other stimulation sites.

Stimulation site	Cluster extent in the PAG (left/right) [number of voxel corresponding to mm^3]	Maximal *t* value (left/right)	Coordinate of peak voxel (*xyz* in MNI space; left/right)
V1	211/977	18.52/18.54	−4,−27,−9/6,−27,−6
V2	42/76	15.43/15.79	−2,−27,−4/6,−29,−8
V3	58/84	12.81/17.41	−4,−35,−8/7,−26,−9
GON	369/458	20.16/21.04	−4,−24,−5/5,−25,−4

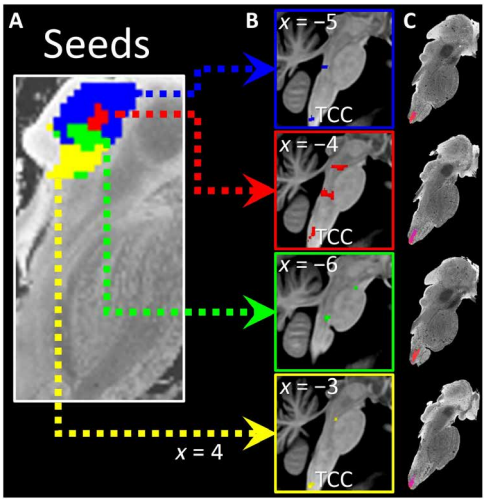

Fig. 3. Downstream functional connectivity from PAG to the trigeminal cervical complex (TCC) in the brainstem. Functional connectivity from (**A**) individual somatotopic clusters of the contralateral PAG (V1: red; V2: green, V3: yellow; GON: blue) to (**B**) the trigeminal cervical complex (TCC). A detailed high-resolution atlas (*68*) of the human brainstem with marked TCC (spinal trigeminal nucleus in pink and spinal trigeminal tract in red) in the respective sagittal slice is presented in (**C**).

the body but in survival-relevant situations. The DPMS is shaped by evolution to reduce acute pain in extreme situations and thus allows the organism survival-relevant activities despite severe injuries. In such extreme situations, the body is flooded by endorphins and activation of the DPMS prompting analgesia allows the chance to survival. In such a situation, one would expect any nociceptive input to be blocked from conscious perception and that this is not restricted to special body parts or indeed low versus intense input. It is self-understood that such situations elude themselves from investigation. However, the fact that the PAG shows a somatotopic arrangement probably enables this structure to attenuate pain specifically in individual dermatomes in less survival-relevant situations. Nevertheless, the PAG might be able to provide both body part–specific and general modulatory output. In animal (*55*) and human studies (*56*), the PAG is activated bilaterally, if the noxious input is big enough, which would, in these circumstances, probably allow for a systemic reaction. One could argue that we have only shown this somatotopic representation for the innervation of the head, e.g., the trigeminal and occipital input, and that we cannot generalize this finding, despite a partitioning even down to individual branches of the trigeminal nerve, to the rest of the body. Investigating the trigeminal system has the advantage that the first relay station of the stimulated peripheral nerve in the central nervous system (here: TCC) as well as the PAG lay within the field of view (FOV) of the imaging. Future work needs to unravel this aspect and also to investigate the functional consequences of such a distribution of the PAG, i.e., to what extent such a specific somatotopy allocates antinociceptive modulation down to individual nerve distribution. The periaqueductal gray contains a precise somatotopy, suggesting that its analgesic effects in response to painful input may be rather specific down to the level of individual dermatomes at least in nonsurvival-relevant situations.

Table 2. Results of the psychophysiological interaction analyses (PPI). Downstream functional connectivity of the contralateral periaqueductal gray to the nuclei of the trigeminal nerve.

Stimulation site	Cluster extent of the functionally connected region in the brainstem [number of voxel corresponding to mm^3]	Maximal *t* value	Coordinate of peak voxel (*xyz* in MNI space)
V1	106	4.02	−3,−47,−62
	774	4.55	−8,−44,−37
	5	2.56	−3,−40,−32
	8	2.58	9,−38,−24
	108	3.47	−4,−30,−20
V2	44	3.20	8,−35,−42
	5	2.60	−5,−44,−41
	46	2.98	7,−44,−38
	26	3.05	−7,−37,−39
	8	2.68	−8,−19,−20
V3	29	3.24	−3,−48,−67
	87	3.90	7,−40,−40
	47	3.23	6,−26,−28
	32	3.04	−5,−32,−26
GON	9	3.06	−5,−48,−66
	31	3.18	1,−39,−63
	32	3.00	−3,−41,−33

MATERIALS AND METHODS

Preregistration

This study was preregistered on 26 June 2019 (title: "Brainstem Mapping of Nociceptive Trigeminal Input") on clinicaltrials.gov: NTC03999060 as an independent secondary outcome. All preregistered primary outcomes (i.e., somatotopic arrangement in brainstem, thalamus, and insular cortex) passed the preregistered statistical thresholds, are published elsewhere (*57*), and are not part of the current manuscript.

Patient consent

The study was approved by the local ethics committee in Hamburg, Germany (PV 5490) and was conducted in accordance with the Declaration of Helsinki. Written informed consent was obtained before initiation of the first study session. Participants could discontinue the study at any time.

Subjects and experimental design

Sixty-three healthy, right-handed volunteers participated in our study on repetitive, randomized, peripheral, painful electrical stimulation of the three trigeminal branches (V1, V2, and V3) innervating the facial dermatomes and the greater occipital nerve (GON) that innervates the back of the head (Fig. 1B). For the primary outcomes (confirmation of earlier studies showing somatotopic representation for the insula, thalamus, etc.), which are not part of this manuscript, we initially measured 25 participants for hypothesis generation. Power calculations revealed that 36 participants were needed to reproduce the hypothesized results. As the results in the PAG, which we present here, are preregistered as secondary outcome, we combined both groups for a robust outcome resulting in 63 participants. Two volunteers of the second cohort had to be excluded due to technical problems, leaving 61 (27 male, age: 28.51 ± 9.4 years) for further analysis. All participants were free from psychiatric and neurological diseases and neither they nor their first-degree relatives suffered from headache disorders.

Electrical stimulation was delivered with an MR-compatible Digitimer DS7A Current Stimulator (Digitimer Ltd., Welwyn Garden City, UK), which was coupled to four WASP electrodes (Specialty Developments, Bexley, UK) via a D188 Remote Electrode Selector (Digitimer Ltd., Welwyn Garden City, UK) and custom-build MR-compatible cables. The cables were built using a published (*58*) and MR-safety tested design to prevent tissue damage due to currents induced by electromagnetic wave coupling. While the subject was sitting on the MR bed, the four electrodes were positioned on the left side according to the three branches of the trigeminal nerve and the GON (Fig. 1B). The GON was located by palpation according to validated procedures (*59*) and the electrode positioned immediately above. V1 was stimulated by means of an electrode placed on an arbitrary vertical line between the medial and lateral quarter of the face, corresponding to the middle of the eyebrow and approximately 1 cm above. The V2 was stimulated 1 cm lateral of the same arbitrary vertical line on the level of a horizontal line through the inferior part of left ala of the nose. V3 was stimulated along the same vertical line approximately 1 cm caudal from the corner of the mouth. Figure 1B sketches the location of the electrodes. Electrode 3 stimulating the third branch of the trigeminal nerve proved to be the most painful of all three trigeminal dermatomes. To make sure that all four sites received robust but bearable pain with the same standardized input, we used this site as orientation for the stimulus intensity.

After fixing the electrodes, the subjects were moved into the scanner and the EDT by means of the QUEST procedure (*60*) at all electrode sites determined. The final current was set to 10 times the EDT of the electrode above V3 for both experiments but was not allowed to exceed 5 mA or a pain rating above 50 (with levels from 0 to 100) for a single pulse. The actual stimulation consisted of a small train of three pulses separated by 100 ms each with 400 V and 2 ms duration. Each stimulus was followed by a break of 3 s (jittered between 2 and 4 s), a pain intensity rating on a visual analog scale (VAS) with levels between 0 and 100 using a button box with the right hand, and another break before the next trial started. For technical reasons, the VAS ratings are only available for the second cohort, i.e., 36 participants. The inter-trial interval was set to 15 s (jittered between 12 and 18 s). The stimulation site was randomized and each site was repeated 10 times per session. The volunteers participated in three sessions resulting in 30 trials per stimulation site and subject during approximately 30 min of functional magnetic resonance imaging (fMRI) scanning. The experimental design is sketched in Fig. 1A.

MR data acquisition and processing

All MR data were recorded with a Siemens 3-T PRISMA scanner (Siemens, Erlangen) using a 64-channel head coil. During the actual experiment, we recorded three sessions with 230 images each using an EPI protocol (repetition time, 2.93 s; echo time, 33 ms; $1.3 \times 1.3 \times 2.0$ mm^3 spatial resolution; GRAPPA acceleration; flip angle, 80°; 72 slices with a multiband factor of 2; FOV, 215 mm; no gap; flow rephasing) with an FOV covering the brainstem as low as C2/3, cerebellum, midbrain, and the insula cortices. In each session, the first five images were removed to avoid scanner saturation effect. Afterward, we recorded fieldmaps (repetition time, 0.792 s; echo times, 5.51 and 7.97 ms; $3 \times 3 \times 2$ mm^3 spatial resolution; flip angle, 20°; 72 slices; FOV 222 mm; no gap) covering the same volume as the EPIs to attenuate the inhomogeneity of the magnetic field. Pulse and breathing were recorded simultaneously to attenuate extracerebral (i.e., cardiovascular) artifacts. Last, we acquired high-resolution (1 mm^3) anatomical images (MPRAGE; repetition time, 2.3 s; echo time, 2.98 ms; flip angle, 9°; 240 slices; FOV, 256 mm).

All MRI data were first filtered using the spatially adaptive nonlocal means filter implemented in the CAT12 toolbox. The fMRI data were then corrected for movements and for distortions of the homogeneity of the magnetic field (fieldmaps) using the realign and unwarp algorithm as implemented in SPM12. In addition, slice time correction was performed using the onsets of the single slices as suited for our multiband protocol. We then calculated a subject-wise general linear model (GLM) including condition-wise onsets of each stimulus as stick functions, which were then convolved with a hemodynamic response function. The button box responses as well as the onset and duration of the VAS were modeled as regressors of no interest. Additional regressors of no interest were included to correct for (uncorrelated) movement, cardiovascular influence, using the algorithms proposed by Deckers *et al.* (*61*), and changes in the spinal fluid extracted from the fourth ventricle. The coregistered structural images were segmented with the unified segmentation approach algorithm implemented in SPM12 but using the templates provided by Blaiotta *et al.* (*62*), which are optimized for the brainstem and spinal cord, to gain deformation fields used to warp the contrast images of the subject-wise GLM into Montreal Neurological Institute (MNI) space. Each step was carefully controlled by

visual inspection. We further calculated a group template, and gray and white matter masks from the warped structural images.

Statistical analysis

Group statistics were calculated by a one-way within-subject analysis of variance (ANOVA) for the whole brain. Significant voxel had to pass a statistical threshold of $p_{FWE} < 0.0001$ (whole brain voxel-wise FWE corrected, $t > 6.5$, $n = 61$, df = 180). Results from the effect of the individual stimulation locations were afterward masked with a PAG mask stemming from Faull *et al.* (*63*), which includes 2,573 voxels in the isotropic 1-mm^3 space. This resulted in four statistical parametric maps, one for each stimulation site, including their voxel-wise *t* values. For each voxel within this PAG mask (Fig. 1C), we then searched for the stimulation site with the maximal *t* value, which resulted in clusters specific for the individual stimulation site within the PAG. The number of voxels within each cluster was then counted.

Functional connectivity with generalized psychophysiological interaction

We estimated the functional connectivity as an exploratory analysis between the resulting individual clusters within the PAG with a psychophysiological interaction (PPI). Because we had four different stimulations, and the current implementation of PPI in the software package SPM12 is only capable to analyze a contrast between two conditions, we used a validated generalized approach for this analysis [generalized psychophysiological interaction (gPPI)] (*64*). Functional connectivity results from the gPPI from the PAG downstream to the brainstem were masked by a brainstem mask (Fig. 1C) and thresholded at $P < 0.01$ (one-sided, *t* test, uncorrected, *t* value > 2.39, $n = 61$, df = 60) and a minimum cluster extent of 5 voxels (i.e., 5 mm^2) for each stimulation site individually. A threshold of $P = 0.01$ is commonly accepted for PPI analysis and indeed an FWE-corrected result is due to the nature of the PPI for such analysis unlikely (*65*–*67*). As the signal in deep brainstem areas is much lower than that for cortical areas and the expected clusters of activation within the trigeminal nerve are very small, we used this liberal threshold.

REFERENCES AND NOTES

1. M. M. Heinricher, H. L. Fields, Central nervous system mechanisms of pain modulation, in *Wall and Melzack's Textbook of Pain*, S. B. McMahon, M. Koltzenburg, I. Tracey, D. Turk, Eds. (Elsevier/Saunders, 6th ed., 2013), pp. 129–142.
2. F. Eippert, J. Finsterbusch, U. Bingel, C. Büchel, Direct evidence for spinal cord involvement in placebo analgesia. *Science* **326**, 404 (2009).
3. M. K. A. Welch, P. J. Goadsby, Chronic daily headache: Nosology and pathophysiology. *Curr. Opin. Neurol.* **15**, 287–295 (2002).
4. K. S. Hemington, M.-A. Coulombe, The periaqueductal gray and descending pain modulation: Why should we study them and what role do they play in chronic pain? *J. Neurophysiol.* **114**, 2080–2083 (2015).
5. D. S. Baskin, W. R. Mehler, Y. Hosobuchi, D. E. Richardson, J. E. Adams, M. A. Flitter, Autopsy analysis of the safety, efficacy and cartography of electrical stimulation of the central gray in humans. *Brain Res.* **371**, 231–236 (1986).
6. D. V. Reynolds, Surgery in the rat during electrical analgesia induced by focal brain stimulation. *Science* **164**, 444–445 (1969).
7. T. L. Yaksh, N. R. F. Al-Rodhan, T. S. Jensen, Sites of action of opiates in production of analgesia, in *Progress in Brain Research*, H. L. Fields, J.-M. Besson, Eds. (Elsevier, 1988), vol. 77, pp. 371–394.
8. A. J. Beitz, The organization of afferent projections to the midbrain periaqueductal gray of the rat. *Neuroscience* **7**, 133–159 (1982).
9. K. A. Keay, K. Feil, B. D. Gordon, H. Herbert, R. Bandler, Spinal afferents to functionally distinct periaqueductal gray columns in the rat: An anterograde and retrograde tracing study. *J. Comp. Neurol.* **385**, 207–229 (1997).
10. X. An, R. Bandler, D. Öngür, J. L. Prince, Prefrontal cortical projections to longitudinal columns in the midbrain periaqueductal gray in Macaque monkeys. *J. Comp. Neurol.* **401**, 455–479 (1998).
11. N. S. Floyd, J. L. Price, A. T. Ferry, K. A. Keay, R. Bandler, Orbitomedial prefrontal cortical projections to distinct longitudinal columns of the periaqueductal gray in the rat. *J. Comp. Neurol.* **422**, 556–578 (2000).
12. T. A. Rizvi, M. Ennis, M. M. Behbehani, M. T. Shipley, Connections between the central nucleus of the amygdala and the midbrain periaqueductal gray: Topography and reciprocity. *J. Comp. Neurol.* **303**, 121–131 (1991).
13. A. A. Cameron, I. A. Khan, K. N. Westlund, K. D. Cliffer, W. D. Willis, The efferent projections of the periaqueductal gray in the rat: A *Phaseolus vulgaris*-leucoagglutinin study. I. Ascending projections. *J. Comp. Neurol.* **351**, 568–584 (1995).
14. J. A. Coffield, K. K. Bowen, V. Miletic, Retrograde tracing of projections between the nucleus submedius, the ventrolateral orbital cortex, and the midbrain in the rat. *J. Comp. Neurol.* **321**, 488–499 (1992).
15. M. S. Fanselow, The midbrain periaqueductal gray as a coordinator of action in response to fear and anxiety, in *The Midbrain Periaqueductal Gray Matter: Functional, Anatomical, and Neurochemical Organization*, A. Depaulis, R. Bandler, Eds. (Springer US, 1991). *NATO ASI Series*, pp. 151–173.
16. E. J. Kim, O. Horovitz, B. A. Pellman, L. M. Tan, Q. Li, G. Richter-Levin, J. J. Kim, Dorsal periaqueductal gray-amygdala pathway conveys both innate and learned fear responses in rats. *Proc. Natl. Acad. Sci. U.S.A.* **110**, 14795–14800 (2013).
17. D. Mobbs, P. Petrovic, J. L. Marchant, D. Hassabis, N. Weiskopf, B. Seymour, R. J. Dolan, C. D. Frith, When fear is near: Threat imminence elicits prefrontal-periaqueductal gray shifts in humans. *Science* **317**, 1079–1083 (2007).
18. P. Carrive, The periaqueductal gray and defensive behavior: Functional representation and neuronal organization. *Behav. Brain Res.* **58**, 27–47 (1993).
19. B. M. D. Oca, J. P. DeCola, S. Maren, M. S. Fanselow, Distinct regions of the periaqueductal gray are involved in the acquisition and expression of defensive responses. *J. Neurosci.* **18**, 3426–3432 (1998).
20. O. K. Faull, M. Jenkinson, M. Ezra, K. T. Pattinson, Conditioned respiratory threat in the subdivisions of the human periaqueductal gray. *eLife* **5**, e12047 (2016).
21. A. B. Satpute, T. D. Wager, J. Cohen-Adad, M. Bianciardi, J.-K. Choi, J. T. Buhle, L. L. Wald, L. F. Barrett, Identification of discrete functional subregions of the human periaqueductal gray. *Proc. Natl. Acad. Sci. U.S.A.* **110**, 17101–17106 (2013).
22. M. Ezra, O. K. Faull, S. Jbabdi, K. T. Pattinson, Connectivity-based segmentation of the periaqueductal gray matter in human with brainstem optimized diffusion MRI. *Hum. Brain Mapp.* **36**, 3459–3471 (2015).
23. F. Benedetti, C. Arduino, M. Amanzio, Somatotopic activation of opioid systems by target-directed expectations of analgesia. *J. Neurosci.* **19**, 3639–3648 (1999).
24. W. Penfield, E. Boldrey, Somatic motor and sensory representation in the cerebral cortex of man as studied by electrical stimulation. *Brain* **60**, 389–443 (1937).
25. U. Bingel, J. Lorenz, V. Glauche, R. Knab, J. Gläscher, C. Weiller, C. Büchel, Somatotopic organization of human somatosensory cortices for pain: A single trial fMRI study. *Neuroimage* **23**, 224–232 (2004).
26. F. Mancini, P. Haggard, G. D. Iannetti, M. R. Longo, M. I. Sereno, Fine-grained nociceptive maps in primary somatosensory cortex. *J. Neurosci.* **32**, 17155–17162 (2012).
27. A.-C. Schmid, J.-H. Chien, J. D. Greenspan, I. Garonzik, N. Weiss, S. Ohara, F. A. Lenz, Neuronal responses to tactile stimuli and tactile sensations evoked by microstimulation in the human thalamic principal somatic sensory nucleus (ventral caudal). *J. Neurophysiol.* **115**, 2421–2433 (2016).
28. J. C. Brooks, L. Zambreanu, A. Godinez, A. D. Craig, I. Tracey, Somatotopic organisation of the human insula to painful heat studied with high resolution functional imaging. *Neuroimage* **27**, 201–209 (2005).
29. L. A. Henderson, S. C. Gandevia, V. G. Macefield, Somatotopic organization of the processing of muscle and cutaneous pain in the left and right insula cortex: A single-trial fMRI study. *Pain* **128**, 20–30 (2007).
30. L. Mazzola, J. Isnard, R. Peyron, M. Guénot, F. Mauguière, Somatotopic organization of pain responses to direct electrical stimulation of the human insular cortex. *Pain* **146**, 99–104 (2009).
31. W. Y. Soper, R. Melzack, Stimulation-produced analgesia: Evidence for somatotopic organization in the midbrain. *Brain Res.* **251**, 301–311 (1982).
32. P. Barbaresi, E. Mensà, Connections from the rat dorsal column nuclei (DCN) to the periaqueductal gray matter (PAG). *Neurosci. Res.* **109**, 35–47 (2016).
33. M. Wiberg, J. Westman, A. Blomqvist, Somatosensory projection to the mesencephalon: An anatomical study in the monkey. *J. Comp. Neurol.* **264**, 92–117 (1987).
34. R. G. Bittar, D. Nandi, H. Carter, T. Z. Aziz, Somatotopic organization of the human periventricular gray matter. *J. Clin. Neurosci.* **12**, 240–241 (2005).
35. E. A. C. Pereira, S. Wang, S. L. F. Owen, T. Z. Aziz, A. L. Green, Human periventricular grey somatosensory evoked potentials suggest rostrocaudally inverted somatotopy. *Stereotact. Funct. Neurosurg.* **91**, 290–297 (2013).
36. F. A. Tinoco Mendoza, T. E. S. Hughes, R. V. Robertson, L. S. Crawford, N. Meylakh, P. M. Macey, V. G. Macefield, K. A. Keay, L. A. Henderson, Detailed organisation of the human midbrain periaqueductal grey revealed using ultra-high field magnetic resonance imaging. *Neuroimage* **266**, 119828 (2023).

37. T. Bartsch, P. J. Goadsby, The trigeminocervical complex and migraine: Current concepts and synthesis. *Curr. Pain Headache Rep.* **7**, 371–376 (2003).
38. L. H. Schulte, C. Sprenger, A. May, Physiological brainstem mechanisms of trigeminal nociception: An fMRI study at 3T. *Neuroimage* **124**, 518–525 (2016).
39. L. H. Schulte, A. May, The migraine generator revisited: Continuous scanning of the migraine cycle over 30 days and three spontaneous attacks. *Brain* **139**, 1987–1993 (2016).
40. H. Basedau, A. May, J. Mehnert, Cerebellar somatotopy of the trigemino-cervical complex during nociception. *Eur. J. Pain*, ejp.2212 (2023).
41. M. H. Schieber, L. S. Hibbard, How somatotopic is the motor cortex hand area? *Science* **261**, 489–492 (1993).
42. M. H. Schieber, Somatotopic gradients in the distributed organization of the human primary motor cortex hand area: Evidence from small infarcts. *Exp. Brain Res.* **128**, 139–148 (1999).
43. P. Hluštík, A. Solodkin, R. P. Gullapalli, D. C. Noll, S. L. Small, Somatotopy in human primary motor and somatosensory hand representations revisited. *Cereb. Cortex* **11**, 312–321 (2001).
44. E. B. Plow, P. Arora, M. A. Pline, M. T. Binenstock, J. R. Carey, Within-limb somatotopy in primary motor cortex—Revealed using fMRI. *Cortex* **46**, 310–321 (2010).
45. J. Lei, T. Sun, B. M. Lumb, H.-J. You, Roles of the periaqueductal gray in descending facilitatory and inhibitory controls of intramuscular hypertonic saline induced muscle nociception. *Exp. Neurol.* **257**, 88–94 (2014).
46. G. G. Pelosi, R. F. Tavares, F. M. A. Corrêa, Rostrocaudal somatotopy in the neural connections between the lateral hypothalamus and the dorsal periaqueductal gray of the rat brain. *Cell. Mol. Neurobiol.* **26**, 633–641 (2006).
47. S. Warren, R. P. Yezierski, N. F. Capra, Chapter 18—The somatosensory system II: Nociception, thermal sense, and touch, in *Fundamental Neuroscience for Basic and Clinical Applications (Fifth Edition)*, D. E. Haines, G. A. Mihailoff, Eds. (Elsevier, 2018), pp. 258–277.e1.
48. A. F. M. DaSilva, L. Becerra, N. Makris, A. M. Strassman, R. G. Gonzalez, N. Geatrakis, D. Borsook, Somatotopic activation in the human trigeminal pain pathway. *J. Neurosci.* **22**, 8183–8192 (2002).
49. M. F. P. Peres, M. A. Stiles, H. C. Siow, T. D. Rozen, W. B. Young, S. D. Silberstein, Greater occipital nerve blockade for cluster headache. *Cephalalgia* **22**, 520–522 (2002).
50. T. P. Jürgens, P. Müller, H. Seedorf, J. Regelsberger, A. May, Occipital nerve block is effective in craniofacial neuralgias but not in idiopathic persistent facial pain. *J. Headache Pain* **13**, 199–213 (2012).
51. L. E. Inan, N. Inan, Ö. Karadaş, H. L. Gül, A. K. Erdemoğlu, Y. Türkel, A. Akyol, Greater occipital nerve blockade for the treatment of chronic migraine: A randomized, multicenter, double-blind, and placebo-controlled study. *Acta Neurol. Scand.* **132**, 270–277 (2015).
52. S. Zhou, N. Hussain, A. Abd-Elsayed, R. Boulos, M. Hakim, M. Gupta, T. Weaver, Peripheral nerve stimulation for treatment of headaches: An evidence-based review. *Biomedicine* **9**, 1588 (2021).
53. J. Hoffmann, J. Mehnert, E. M. Koo, A. May, Greater occipital nerve block modulates nociceptive signals within the trigeminocervical complex. *J Neurol Neurosurg Psychiatry* **92**, 1335–1340 (2021).
54. H. Basedau, T. Nielsen, K. Asmussen, K. Gloss, J. Mehnert, R. H. Jensen, A. May, Experimental evidence of a functional relationship within the brainstem trigeminocervical complex in humans. *Pain* **163**, 729–734 (2022).
55. R. Levine, M. M. Morgan, J. T. Cannon, J. C. Liebeskind, Stimulation of the periaqueductal gray matter of the rat produces a preferential ipsilateral antinociception. *Brain Res.* **567**, 140–144 (1991).
56. S. La Cesa, E. Tinelli, N. Toschi, G. Di Stefano, S. Collorone, A. Aceti, A. Francia, G. Cruccu, A. Truini, F. Caramia, fMRI pain activation in the periaqueductal gray in healthy volunteers during the cold pressor test. *Magn. Reson. Imaging* **32**, 236–240 (2014).
57. J. Mehnert, H. Basedau, L.-M. Sturm, T. Nielsen, R. H. Jensen, A. May, Functional brainstem representations of the human trigeminal cervical complex. *Cephalalgia* **43**, 033310242311748 (2023).
58. K. Schmidt, K. Forkmann, C. Sinke, M. Gratz, A. Bitz, U. Bingel, The differential effect of trigeminal vs. peripheral pain stimulation on visual processing and memory encoding is influenced by pain-related fear. *Neuroimage* **134**, 386–395 (2016).
59. M. Loukas, A. El-Sedfy, R. S. Tubbs, R. G. Louis, C. H. T. Wartmann, B. Curry, R. Jordan, Identification of greater occipital nerve landmarks for the treatment of occipital neuralgia. *Folia Morphol.* **65**, 337–342 (2006).
60. P. Taesler, M. Rose, Psychophysically-anchored, robust thresholding in studying pain-related lateralization of oscillatory prestimulus activity. *J. Vis. Exp.*, 55228 (2017).
61. R. H. R. Deckers, P. van Gelderen, M. Ries, O. Barret, J. H. Duyn, V. N. Ikonomidou, M. Fukunaga, G. H. Glover, J. A. de Zwart, An adaptive filter for suppression of cardiac and respiratory noise in MRI time series data. *Neuroimage* **33**, 1072–1081 (2006).
62. C. Blaiotta, P. Freund, M. J. Cardoso, J. Ashburner, Generative diffeomorphic modelling of large MRI data sets for probabilistic template construction. *Neuroimage* **166**, 117–134 (2018).
63. O. K. Faull, M. Jenkinson, S. Clare, K. T. S. Pattinson, Functional subdivision of the human periaqueductal grey in respiratory control using 7 tesla fMRI. *Neuroimage* **113**, 356–364 (2015).
64. D. G. McLaren, M. L. Ries, G. Xu, S. C. Johnson, A generalized form of context-dependent psychophysiological interactions (gPPI): A comparison to standard approaches. *Neuroimage* **61**, 1277–1286 (2012).
65. P. Das, A. H. Kemp, B. J. Liddell, K. J. Brown, G. Olivieri, A. Peduto, E. Gordon, L. M. Williams, Pathways for fear perception: Modulation of amygdala activity by thalamo-cortical systems. *Neuroimage* **26**, 141–148 (2005).
66. D. Sharoh, T. van Mourik, L. J. Bains, K. Segaert, K. Weber, P. Hagoort, D. G. Norris, Laminar specific fMRI reveals directed interactions in distributed networks during language processing. *Proc. Natl. Acad. Sci. U.S.A.* **116**, 21185–21190 (2019).
67. J. Kim, B. Horwitz, Investigating the neural basis for fMRI-based functional connectivity in a blocked design: Application to interregional correlations and psycho-physiological interactions. *Magn. Reson. Imaging* **26**, 583–593 (2008).
68. S. M. Adil, E. Calabrese, L. T. Charalambous, J. J. Cook, S. Rahimpour, A. F. Atik, G. P. Cofer, B. A. Parente, G. A. Johnson, S. P. Lad, L. E. White, A high-resolution interactive atlas of the human brainstem using magnetic resonance imaging. *Neuroimage* **237**, 118135 (2021).

Acknowledgments

Funding: This study was funded by the Deutsche Forschungsgemeinschaft (DFG, German Research Foundation-SFB 936) 178316478/A5 to A.M. and by the Deutsche Forschungsgemeinschaft (DFG, German Research Foundation) TI 1110/1 and the Max Planck Society to A.T. **Author contributions:** J.M.: Data analysis, data interpretation, and drafting and writing of the manuscript. A.T.: Data analysis and writing of the manuscript. H.B.: Data acquisition and analysis and writing of the manuscript. A.M.: Drafting of the study, data analysis, data interpretation, and drafting and writing of the manuscript. **Competing interests:** The authors declare that they have no competing interests. **Data and materials availability:** All data needed to evaluate the conclusions in the paper are present in the paper. Therefore, all deidentified imaging raw data and variables, involving the documentation of the processing procedure, are available on https://doi.org/10.5061/dryad.mw6m90642.

Submitted 18 July 2023
Accepted 13 February 2024
Published 20 March 2024
10.1126/sciadv.adj8213